J|A|C|S
ARTICLES
Published on Web 07/31/2002

Photofragment Translational Spectroscopy of 1,3-Butadiene and 1,3-Butadiene-1,1,4,4-d_4 at 193 nm

Jason C. Robinson, Sean A. Harris, Weizhong Sun,† Niels E. Sveum, and Daniel M. Neumark*

Contribution from the Chemical Sciences Division, Lawrence Berkeley National Laboratory, Berkeley, California 94720, and Department of Chemistry, University of California, Berkeley, California 94720

Received December 19, 2001

Abstract: The photodissociation dynamics of 1,3-butadiene at 193 nm have been investigated with photofragment translational spectroscopy coupled with product photoionization using tunable VUV synchrotron radiation. Five product channels are evident from this study: $C_4H_5 + H$, $C_3H_3 + CH_3$, $C_2H_3 + C_2H_3$, $C_4H_4 + H_2$, and $C_2H_4 + C_2H_2$. The translational energy ($P(E_T)$) distributions suggest that these channels result from internal conversion to the ground electronic state followed by dissociation. To investigate the dissociation dynamics in more detail, further studies were carried out using 1,3-butadiene-1,1,4,4-d_4. Branching ratios were determined for the channels listed above, as well as relative branching ratios for the isotopomeric species produced from 1,3-butadiene-1,1,4,4-d_4 dissociation. $C_3H_3 + CH_3$ is found to be the dominant channel, followed by $C_4H_5 + H$ and $C_2H_4 + C_2H_2$, for which the yields are approximately equal. The dominance of the $C_3H_3 + CH_3$ channel shows that isomerization to 1,2-butadiene followed by dissociation is facile.

Introduction

The photophysics and photochemistry of conjugated polyenes represent a fruitful and challenging area of interaction between chemical physics and physical organic chemistry. The simplest of these, 1,3-butadiene, has been studied using an impressive array of experimental and theoretical techniques.[1,2] Its electronic spectrum and short-time dynamics following photoexcitation have been investigated with frequency- and time-domain absorption spectroscopy, as well as resonance Raman spectroscopy. This experimental work combined with recent electronic structure calculations of the ground- and excited-state potential energy surfaces has led to a reasonably clear understanding of the nature of the electronic states involved in the initial excitation and early-time dynamics. On the other hand, nearly all studies of 1,3-butadiene photochemistry have been performed either in solution or in the gas phase under multiple-collision conditions; a systematic study of the primary photoproducts under collisionless conditions has never been undertaken. In this paper, we investigate the photodissociation dynamics at 193 nm of 1,3-butadiene using molecular beam photofragment translational spectroscopy, with the goal of identifying the primary products and determining the mechanism for each of the observed product channels.

Figure 1 shows the energetically accessible products from 1,3-butadiene photodissociation at 193 nm. The energetics were obtained from previously determined experimental and theoretical heats of formation (298 K values were used for consistency).[3−10] Several radical channels and molecular channels are accessible. In addition, there are low-lying structural isomers of 1,3-butadiene not shown in Figure 1, namely, 1,2-butadiene,

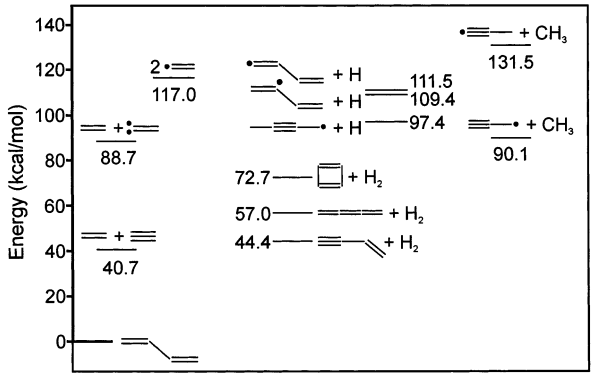

Figure 1. Energy level diagram for possible product channels following 193-nm excitation of 1,3-butadiene. Solid black circles indicate radical sites. Heats of formation at 298 K were used to determine energetics.

* Author to whom correspondence should be addressed: E-mail: dan@radon.cchem.berkeley.edu.

† Present address: AXT, Inc., Fremont, CA 94538.

(1) Orlandi, G.; Zerbetto, F.; Zgierski, M. Z. *Chem. Rev.* **1991**, *91*, 867−891.
(2) McDiarmid, R. *Adv. Chem. Phys.* **1999**, *110*, 177−214.
(3) Nguyen, T. T.; King, K. D. *Int. J. Chem. Kinet.* **1982**, *14*, 613−621.
(4) Lias, S. G.; Bartmas, J. E.; Liebman, J. F.; Holmes, J. L.; Levin, R. D.; Mallard, W. G. *J. Phys. Chem. Ref. Data* **1988**, 117.
(5) Ervin, K. M.; Gronert, S.; Barlow, S. E.; Gilles, M. K.; Harrison, A. G.; Bierbaum, V. M.; DePuy, C. H.; Lineberger, W. C.; Ellison, G. B. *J. Am. Chem. Soc.* **1990**, *112*, 5750−5759.
(6) Miller, J. A.; Melius, C. F. *Combust. Flame* **1992**, *91*, 21−39.
(7) Parker, C. L.; Cooksy, A. L. *J. Phys. Chem. A* **1999**, *103*, 2160−2169.
(8) Robinson, M. S.; Polak, M. L.; Bierbaum, V. M.; DePuy, C. H.; Lineberger, W. C. *J. Am. Chem. Soc.* **1995**, *117*, 6766−6778.
(9) Gilbert, T.; Pfab, R.; Fischer, I.; Chen, P. *J. Chem. Phys.* **2000**, *112*, 2575−2578.
(10) *NIST Chemistry Webbook*, 2002.

cyclobutene, and bicyclobutane. Hence, the photochemistry and dissociation/isomerization dynamics of 1,3-butadiene are expected to be quite complex.

The electronic spectrum of *s-trans*-1,3-butadiene in the region probed by our experiment has been of interest for many years. There is a strong $\pi^* \rightarrow \pi$ transition, the $1^1B_u-1^1A_g$ band, beginning around 46 000 cm^{-1} (217 nm) and composed of several diffuse vibrational bands, as well as a much sharper feature at 50 574 cm^{-1} from a vibronically allowed transition to the ^1B_g Rydberg state.[11] Leopold et al.[12] found that even when the butadiene was cooled in a free-jet expansion, the features of the $1^1B_u-1^1A_g$ band remained diffuse, with line widths of several hundred reciprocal centimeters, suggesting extremely rapid radiationless decay from the 1^1B_u state. Dinur et al.[13] proposed that this decay was associated with coupling between the 1^1B_u state and nearly degenerate 2^1A_g state, an optically inaccessible state that was shown in resonance Raman spectroscopy experiments by Hudson and co-workers[14] to lie slightly below the 1^1B_u state. A series of electronic structure calculations on the excited and ground electronic states by Olivucci,[15] Domcke,[16,17] and others[18−20] demonstrated that the dynamics of 1,3-butadiene after excitation of the 1^1B_u state are dominated by conical intersections, one between the 1^1B_u and 2^1A_g states that causes rapid decay of the 1^1B_u state, and a second between the 2^1A_g and 1^1A_g states, leading to population of the ground electronic state. Recent time-resolved experiments by Assenmacher[21] and Fuss[22] have shown explicitly that the 1^1B_u state decays in less than 50 fs; the latter study yielded multiple time constants that were interpreted in terms of dynamics occurring at the $2^1A_g/1^1A_g$ conical intersection.

The above results regarding the spectroscopy and early-time dynamics of 1,3-butadiene complement a series of earlier experiments in which the products from butadiene photoexcitation and pyrolysis were identified. Studies of 1,3-butadiene photochemistry in hydrocarbon solution showed some cyclobutene formation and a smaller amount of bicyclobutane.[23] Gas-phase studies, in which 1,3-butadiene was dissociated by mercury sensitization[24] or direct UV photolysis,[25−29] showed evidence for two molecular dissociation channels, $C_2H_2 + C_2H_4$ and $C_4H_4 + H_2$, and a radical−radical $CH_3 + C_3H_3$ channel. The C_4H_4 product was tentatively assigned to be vinylacetylene. The radical channel, inferred from mass spectrometry and secondary reaction products, was proposed to arise from isomerization to form vibrationally hot 1,2-butadiene (CH_2═C═CH−CH_3) followed by dissociation to $CH_3 + C_3H_3$. Experiments on 1,3-butadiene-1,1,4,4-d_4 suggested that $C_2H_2 + C_2H_4$ products resulted from formation and decomposition of cyclobutene as well as additional pathways including a four-center hydrogen migration transition state.[27] On the basis of the observation of pressure quenching of the dissociation products, Haller and Srinivasan[26] proposed in 1964 that in the gas-phase photolysis of 1,3-butadiene photoexcitation was followed by rapid internal conversion and dissociation of highly vibrationally excited molecules on the ground electronic state.

High-temperature pyrolysis of 1,3-butadiene was studied in a series of shock tube experiments.[30−35] The earlier experiments were interpreted by Benson[36] and Kiefer[31,32] to indicate that the first step in pyrolysis was dissociation to two vinyl radicals. However, the activation energy for this process had to be around 100 kcal/mol in order to explain the observed early-time kinetics, a value considerably less than the accepted bond dissociation energy of 117 kcal/mol. A more recent study by Hidaka and co-workers,[35] which was analyzed with a kinetic model consisting of 89 reactions, concluded that neither vinyl production nor $C_4H_5 + H$ were important compared to isomerization to 1,2-butadiene followed by dissociation to $CH_3 + C_3H_3$ or compared to the molecular $C_2H_2 + C_2H_4$ channel. On the other hand, in a recent study by Dai and co-workers,[37] emission from vibrationally excited C_2H_3 was observed from photolysis of butadiene at 193 nm.

These photolysis and pyrolysis experiments raise questions about the competition between molecular and radical dissociation channels of 1,3-butadiene and the role of isomerization in the dissociation dynamics. The experiments were conducted at sufficiently high pressure so that secondary reactions of radical products occurred on the time scale of the measurements, meaning that even if vinyl and $C_4H_5 + H$ channels were important, these products would not have been directly detected, except in the experiment by Dai.[37] Therefore, it is worth investigating the dissociation dynamics of 1,3-butadiene under collisionless conditions, in an experiment where all possible channels can be detected on an approximately equal footing. Surprisingly, only one collisionless photodissociation experiment to date has been carried out on this molecule, in which Valentini[38] determined the (v, J) distribution of the H_2 photoproduct from butadiene photolysis at 212.8 nm. We have recently reported results for the collisionless photodissociation of 1,2-butadiene at 193 nm using photofragment translational spectroscopy, in which we found that $CH_3 + C_3H_3$ was the dominant channel accompanied by a small amount of $C_4H_5 + H$; no molecular channels were observed.[39]

(11) McDiarmid, R.; Sheybani, A. H. *J. Chem. Phys.* **1988**, *89*, 1255−1261.
(12) Leopold, D. G.; Pendley, R. D.; Roebber, J. L.; Hemley, R. J.; Vaida, V. *J. Chem. Phys.* **1984**, *81*, 4218−4228.
(13) Dinur, U.; Hemley, R. J.; Karplus, M. *J. Phys. Chem.* **1983**, *87*, 924−932.
(14) Chadwick, R. R.; Zgierski, M. Z.; Hudson, B. S. *J. Chem. Phys.* **1991**, *95*, 7204−7211.
(15) Olivucci, M.; Ragazos, I. N.; Bernardi, F.; Robb, M. A. *J. Am. Chem. Soc.* **1993**, *115*, 3710−3721.
(16) Krawczyk, R. P.; Malsch, K.; Hohlneicher, G.; Gillen, R. C.; Domcke, W. *Chem. Phys. Lett.* **2000**, *320*, 535−541.
(17) Ostojic, B.; Domcke, W. *Chem. Phys.* **2001**, *269*, 1−10.
(18) Ito, M.; Ohmine, I. *J. Chem. Phys.* **1997**, *106*, 3159−3173.
(19) Zilberg, S.; Haas, Y. *J. Phys. Chem. A* **1999**, *103*, 2364−2374.
(20) Sakai, S. *Chem. Phys. Lett.* **2000**, *319*, 687−694.
(21) Assenmacher, F.; Gutmann, M.; Hohlneicher, G.; Stert, V.; Radloff, W. *Phys. Chem. Chem. Phys.* **2001**, *3*, 2981−2982.
(22) Fuss, W.; Schmid, W. E.; Trushin, S. A. *Chem. Phys. Lett.* **2001**, *342*, 91−98.
(23) Leigh, W. J. In *Organic Photochemistry and Photobiology*; Horspool, W. M., Song, P.-S., Eds.; CRC Press: Boca Raton, FL, 1995; pp 123−142.
(24) Collin, J.; Lossing, F. P. *Can. J. Chem.* **1957**, *35*, 778−787.
(25) Srinivasan, R. *Adv. Photochem.* **1966**, *4*, 113−142.
(26) Haller, I.; Srinivasan, R. *J. Chem. Phys.* **1964**, *40*, 1992−1997.
(27) Haller, I.; Srinivasan, R. *J. Am. Chem. Soc.* **1966**, *88*, 3694−3698.
(28) Doepker, R. D. *J. Phys. Chem.* **1968**, *72*, 4037−4042.
(29) Collin, G. J.; Deslauriers, H.; Maré, G. R. D.; Poirer, R. A. *J. Phys. Chem.* **1990**, *94*, 134−141.
(30) Skinner, G. B.; Sokoloski, E. M. *J. Phys. Chem.* **1960**, *64*, 1028−1031.
(31) Kiefer, J. H.; Mitchell, K. I.; Wei, H. C. *Int. J. Chem. Kinet.* **1988**, *20*, 787−809.
(32) Kiefer, J. H.; Wei, H. C.; Kern, R. D.; Wu, C. H. *Int. J. Chem. Kinet.* **1985**, *17*, 225−253.
(33) Kiefer, J. H.; Kumaran, S. S.; Mudipalli, P. S. *Chem. Phys. Lett.* **1994**, *224*, 51−55.
(34) Rao, V. S.; Takeda, K.; Skinner, G. B. *Int. J. Chem. Kinet.* **1988**, *20*, 153−164.
(35) Hidaka, Y.; Higashihara, T.; Ninomiya, N.; Masaoka, H.; Nakamura, T.; Kawano, H. *Int. J. Chem. Kinet.* **1996**, *28*, 137−151.
(36) Benson, S. W.; Haugen, G. R. *J. Phys. Chem.* **1967**, *71*, 1725−1746.
(37) Letendre, L.; Liu, D. K.; Pibel, C. D.; Halpern, J. B.; Dai, H. L. *J. Chem. Phys.* **2000**, *112*, 9209−9212.
(38) Venkataraman, B. K.; Valentini, J. J. *Chem. Phys. Lett.* **1992**, *194*, 191−195.

In the work reported here, we aim to elucidate all of the primary product channels from the 193-nm photolysis of 1,3-butadiene and 1,3-butadiene-1,1,4,4-d_4 under single-collision conditions. To achieve this goal, the technique of molecular photofragment translational spectroscopy has been used to identify the photofragments and ascertain their center-of-mass frame translational energy distributions. While many experiments of this type have been carried out using electron impact ionization of the scattered photoproducts,[40] the extensive dissociative ionization characteristic of electron impact would greatly complicate the analysis of a system as complex as 1,3-butadiene. Therefore, most of these experiments were conducted at the Advanced Light Source (ALS) at the Lawrence Berkeley National Laboratory, using tunable vacuum ultraviolet (VUV) synchrotron radiation to photoionize the products. Using this instrument, complications due to dissociative ionization were mitigated by tuning the photoionization (PI) energy below the dissociative photoionization threshold for each fragment of interest. Furthermore, identification of photoproducts was possible for some channels by measuring photoionization efficiency yields as a function of VUV energy for different fragments. However, the extraction of quantitative branching ratios for the various reaction channels from PI measurements alone requires absolute photoionization cross sections, and these have not been measured for most of the possible products in Figure 1. Therefore, the PI measurements were supplemented by photodissociation measurements on a different instrument in which scattered photoproducts were ionized by electron impact (EI) with high-energy (80 eV) electrons.

We found five primary reaction channels from the 193-nm dissociation of 1,3-butadiene. The observed product channels are loss of atomic hydrogen, methyl, vinyl, molecular hydrogen, and acetylene—the three radical channels and two molecular channels shown in Figure 1—with methyl loss found to be the dominant product channel. A minor sequential-dissociation channel was also identified, corresponding to the loss of an H atom following loss of H_2. Center-of-mass frame translational energy distributions were determined for each of these channels. Further studies were conducted on 1,3-butadiene-1,1,4,4-d_4 to determine the nature of the products and the branching ratios between the possible isotopomeric products for each channel. The translational energy distributions are consistent with ground-state dissociation for all channels, with the methyl and acetylene loss channels most likely occurring via isomerization prior to dissociation. The molecular channels proceed through substantial exit barriers with respect to the separated products, while no such barriers are apparent for the radical channels.

Experiment Section

A. VUV Photoionization Instrument. Two instruments were used in this work—one with VUV PI detection and one with EI detection. The PI instrument has been described in detail elsewhere.[41,42] The specifics of the current experiments are similar to those in a previous experiment probing the photodissociation dynamics of 1,2-butadiene.[39] In brief, a pulsed molecular beam is crossed with a pulsed photolysis laser beam in a rotating source/fixed detector configuration. Scattered photofragments enter a multiply differentially pumped detection region where they are photoionized by VUV light from the ALS; the resulting ions are mass-selected and detected. Photofragment time-of-flight (TOF) distributions are measured at selected scattering angles and VUV wavelengths. Alternatively, the photoionization efficiency (PIE) curve for a particular fragment can be obtained by measuring the mass-selected ion yield as a function of VUV wavelength.

1,3-Butadiene was obtained from Aldrich (99+%) and Scott Specialty Gases (99.0%), and 1,3-butadiene-1,1,4,4-d_4 was obtained from Cambridge Isotope Laboratories (98%). These chemicals were used without further purification. A pulsed molecular beam of ~5% 1,3-butadiene or 1,3-butadiene-1,1,4,4-d_4 in either helium or neon was generated with a pulsed valve operating at 100 Hz. The stagnation pressure was maintained around 400 Torr using a vacuum regulator, and the pulsed valve was heated to ~60 °C to minimize the presence of dimers. The velocity (V_0) of the 1,3-butadiene beam seeded in helium was 1290 m/s with a speed ratio (S) of 11. For 1,3-butadiene-1,1,4,4-d_4 beam seeded in helium, $V_0 = 1290$ m/s and $S = 10$. For the 1,3-butadiene seeded in neon, $V_0 = 790$ m/s and $S = 8.5$. The molecular beam was skimmed twice and crossed with 193-nm light emitted by a Lambda Physik LPX-200 ArF excimer laser. The laser beam was perpendicular to both the molecular beam and detector axes, and the molecular beam source could be rotated about the laser beam with respect to the fixed detector. Laser power was controlled to ensure that the TOF spectra were not the result of multiphoton processes, as confirmed by laser power dependence studies. For TOF studies, the laser was focused to a 2 mm × 4 mm rectangle and the laser pulse energy was maintained around 6 mJ/pulse. Shot-to-shot background subtraction was rendered unnecessary by choosing photoionization energies below the appearance potential of each species from the parent molecule.

Following dissociation, the neutral photofragments traveled 15.1 cm prior to ionization. The scattered neutral photofragments were ionized by tunable VUV undulator radiation from the Chemical Dynamics Beamline at the ALS. The ionized fragments were mass selected by a quadrupole mass filter, and the signal from the fragments of interest was counted as a function of time by a computer-interfaced multichannel scaler (MCS). The ion flight constant for the detector was 5.26 μs amu$^{-1/2}$. An MCS bin width of 2 μs was used for all spectra presented here.

The properties of the VUV undulator radiation used in these experiments for photoionization of the dissociation products were described previously.[43,44] The PIE measurements were conducted at 1.5 or 1.9 GeV electron beam energy, while the TOF spectra were collected using 1.9 GeV electron beam energy. While the VUV photon flux is generally higher at 1.9 GeV, at 1.5 GeV the useable VUV radiation range extends to a lower value, ~5 eV, which is more convenient for photoionization scans of radicals with low ionization potentials. The bandwidth of the radiation from the undulator is ~2.3%. The undulator radiation passes through a differentially pumped gas filter to remove the higher harmonics.[45] In these experiments, the gas filter was maintained at roughly 25 Torr of continuously flowing argon. While the upstream mirrors and the gas filter remove the higher harmonics of the undulator radiation, a small blue tail remains on the fundamental. To reduce the effects of this component of the radiation, an MgF_2 window, which transmits no light above 11.2 eV, could be inserted into the path of the undulator radiation. A calorimeter was employed to continuously monitor the VUV radiation flux.

Angle-resolved TOF spectra were obtained by selecting the mass-to-charge ratio (m/e) for the ion of interest, fixing the source angle,

(39) Robinson, J. C.; Sun, W.; Harris, S. A.; Qi, F.; Neumark, D. M. *J. Chem. Phys.* **2001**, *115*, 8359−8365.
(40) Butler, L. J.; Neumark, D. M. *J. Phys. Chem.* **1996**, *100*, 12801−12816.
(41) Blank, D. A. Ph.D. Thesis, University of California, Berkeley, 1997.
(42) Yang, X.; Blank, D. A.; Lin, J.; Wodtke, A. M.; Suits, A. G.; Lee, Y. T. *Rev. Sci. Instrum.* **1997**, *68*, 3317−3326.
(43) Heimann, P. A.; Koike, M.; Hsu, C. W.; Evans, M.; Ng, C. Y.; Blank, D.; Yang, X. M.; Flaim, C.; Suits, A. G.; Lee, Y. T. *SPIE Proc.* **1996**, *2856*, 90−99.
(44) Koike, M.; Heimann, P. A.; Kung, A. H.; Namioka, T.; Digennaro, R.; Gee, B.; Yu, N. *Nucl. Instrum. Methods Phys. Res. A* **1994**, *347*, 282−286.
(45) Suits, A. G.; Heimann, P.; Yang, X. M.; Evans, M.; Hsu, C. W.; Lu, K. T.; Lee, Y. T.; Kung, A. H. *Rev. Sci. Instrum.* **1995**, *66*, 4841−4844.

and setting the undulator gap to deliver the appropriate photoionization energy. Typically, TOF spectra were obtained at several source angles for each *m*/*e*. PIE curves for specific photofragments were obtained by selecting *m*/*e*, fixing the source angle, and stepping the undulator radiation. In constructing the curve, the scattering signal for each fragment was integrated, background subtracted, and normalized.

B. Electron Impact Instrument. Photodissociation experiments were also carried out on a fixed-source, rotating-detector apparatus featuring EI detection.[46] Most operating conditions were similar to those described above. A pulsed molecular beam of ~5% 1,3-butadiene seeded in helium was generated with a pulsed valve operating at 100 Hz. The stagnation pressure was maintained around 500 Torr using a vacuum regulator. To minimize the presence of dimers, the early part of the beam pulse was selected with a four-slotted (0.5 mm/slot) chopper running at 100 Hz; for this section of the beam, $V_0 = 1240$ m/s and $S = 10$. We also investigated the dissociation of the dimer, using a later part of the beam pulse for which $V_0 = 1340$ m/s. The molecular beam was skimmed twice and crossed with 193-nm light emitted by a Lambda Physik LPX-220i ArF excimer laser. The laser beam was perpendicular to the molecular beam, and the detector could be rotated in the plane defined by the laser beam and the molecular beam source. The laser was focused to a 2 mm × 5 mm rectangle and the laser pulse energy was maintained around 4 mJ/pulse. Shot-to-shot background subtraction was used to remove the contribution from the parent molecular beam. The neutral photofragments traveled 20 cm prior to ionization with ~80-eV electrons. The ionized fragments were mass selected by a quadrupole mass filter, and the signal from the fragments of interest was counted as a function of time by a computer-interfaced MCS. The ion flight constant for the detector was 4.14 μs amu$^{-1/2}$. An MCS bin width of 2 μs was used for the spectra presented here.

Results

A. TOF Spectra Collected Using Photoionization. Guided by Figure 1, product TOF spectra from 1,3-butadiene dissociation on the PI instrument were collected at several laboratory angles for ions with *m*/*e* = 53 ($C_4H_5^+$), 52 ($C_4H_4^+$), 39 ($C_3H_3^+$), 28 ($C_2H_4^+$), 27 ($C_2H_3^+$), 26 ($C_2H_2^+$), and 15 (CH_3^+). Because of the poor kinematics associated with H and H_2 detection, TOF spectra were not obtained for *m*/*e* = 1 or 2. In the following TOF spectra, photoionization energies were chosen to minimize contributions from dissociative ionization (DI) of the parent beam as well as from higher *m*/*e* species. In several cases below, TOF profiles at smaller laboratory angles (i.e., closer to the molecular beam) were taken at lower photoionization energies with the MgF_2 window in place, while at large angles, higher photoionization energies were chosen (often precluding the use of the window). Higher photoionization energies were selected at larger angles since product flux was generally lower and DI of the parent beam does not contribute to these TOF profiles. Generally, the energies selected were near the maximums of the PIE curves, shown in the section, PIE Measurements.

All TOF spectra were collected using molecular beams seeded in He, except for *m*/*e* = 53, where TOF spectra were obtained for both Ne- and He-seeded beams. Experimental details for each TOF spectrum are listed in the figure captions, including the VUV photoionization energy and whether the MgF_2 window was used. Figures 2−4 show TOF spectra nominally attributed to radical photofragments. Figure 2a,b shows TOF spectra for *m*/*e* = 53 ($C_4H_5^+$) at $\Theta_{LAB} = 8°$. Figure 2a shows the TOF spectrum using the He-seeded beam, while Figure 2b presents the TOF spectrum using the Ne-seeded beam. Additional spectra were collected using the He-seeded beam at $\Theta_{LAB} = 6°$ and 10°. TOF spectra are shown for *m*/*e* = 39 ($C_3H_3^+$) at laboratory angles $\Theta_{LAB} = 8°$ and 25° in Figure 3a,b. Additional spectra were collected at laboratory angles $\Theta_{LAB} = 10°$, 15°, and 20°. Figure 3c shows the TOF spectrum for the methyl radical (*m*/*e* = 15; upper right-hand panel) at $\Theta_{LAB} = 15°$. Figure 4a,b shows TOF spectra for *m*/*e* = 27 ($C_2H_3^+$) at scattering angles of $\Theta_{LAB} = 11°$ and 20°; additional TOF spectra were obtained at $\Theta_{LAB} = 8°$ and 15°.

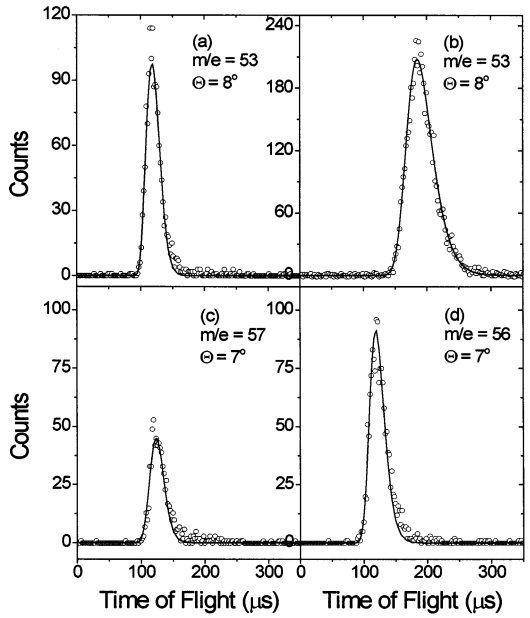

Figure 2. TOF spectra for *m*/*e* = 53 ($C_4H_5^+$) at source angles of 8° from beams seeded in (a) helium and (b) neon using VUV photoionization energies of 8.7 and 8.5 eV, respectively, with the MgF_2 window in the path of the undulator radiation. Also shown are TOF spectra for (c) *m*/*e* = 57 ($C_4D_4H^+$) and (d) *m*/*e* = 56 ($C_4D_3H_2^+$) from 1,3-butadiene-1,1,4,4-d_4 at a source angle of 7° using 8.5 eV with the MgF_2 window. For all TOF spectra, the open circles represent the data and the solid line represents the forward convolution fit to the data using the $P(E_T)$ distribution shown in Figure 9a.

TOF spectra for molecular fragments are shown in Figures 5 and 6. Figure 5a,b presents TOF spectra for *m*/*e* = 52 ($C_4H_4^+$) at laboratory angles $\Theta_{LAB} = 10°$ and 15°. TOF spectra for *m*/*e* = 26 ($C_2H_2^+$) and *m*/*e* = 28 ($C_2H_4^+$) are shown in Figure 6a−c. Additional TOF spectra were obtained for *m*/*e* = 26 at $\Theta_{LAB} = 15°$ and for *m*/*e* = 28 at $\Theta_{LAB} = 15°$. The TOF spectra in Figure 6 are the only spectra collected with photoionization detection that contain two distinct peaks.

As mentioned above, the photoionization energies used in each TOF spectrum were chosen to minimize dissociative ionization of higher mass fragments. Hence, each TOF spectrum should correspond almost entirely to parent ions at the selected *m*/*e*, so that each mass at which signal is observed can be readily identified with a primary reaction channel. Therefore, we have preliminary evidence for all five distinct primary product channels shown in Figure 1:

$$C_4H_6 + h\nu \rightarrow C_4H_5 + H \quad \text{(R1)}$$

$$C_4H_6 + h\nu \rightarrow C_3H_3 + CH_3 \quad \text{(R2)}$$

$$C_4H_6 + h\nu \rightarrow C_2H_3 + C_2H_3 \quad \text{(R3)}$$

$$C_4H_6 + h\nu \rightarrow C_4H_4 + H_2 \quad \text{(R4)}$$

(46) Lee, Y. T.; McDonald, J. D.; LeBreton, P. R.; Herschbach, D. R. *Rev. Sci. Instrum.* **1969**, *40*, 1402−1408.

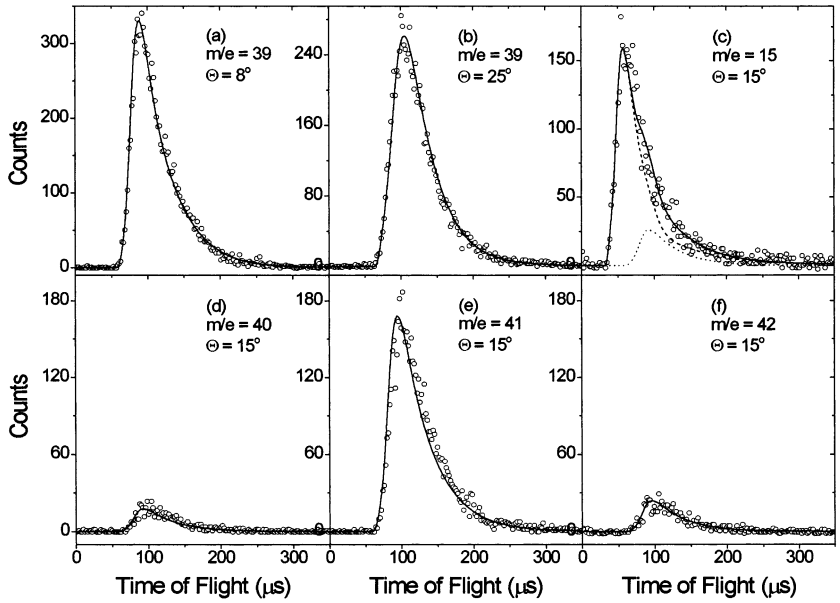

Figure 3. TOF spectra for $m/e = 39$ ($C_3H_3^+$) at source angles of (a) 8° and (b) 25° at 10.0 and 11.0 eV, respectively. The MgF_2 window was in place for the 10.0-eV TOF spectrum. The TOF spectrum for $m/e = 15$ (CH_3^+) at 15° with a photoionization energy of 11.0 eV is shown in (c) and is fit with the same $P(E_T)$ distribution used to fit (a) and (b). The single-dashed line represents the contribution from $m/e = 15$, and the dotted line represents the contribution from dissociative ionization of mass 39 product, the momentum-matched partner to the mass 15 product. Also, TOF spectra are shown for (d) $m/e = 40$ ($C_3DH_2^+$), (e) $m/e = 41$ ($C_3D_2H^+$), and (f) $m/e = 42$ ($C_3D_3^+$) from 1,3-butadiene-1,1,4,4-d_4 at $\Theta_{LAB} = 15°$ using 10.5-eV photoionization energy and the MgF_2 window. For all TOF spectra, the open circles represent the data and the solid line represents the forward convolution fit to the data using the $P(E_T)$ distribution shown in Figure 9b.

$$C_4H_6 + h\nu \rightarrow C_2H_4 + C_2H_2 \qquad \text{(R5)}$$

To unravel the mechanisms leading to production of the five channels, TOF spectra from the photodissociation of 1,3-butadiene-1,1,4,4-d_4 were collected. Reaction R1, H atom elimination, was further investigated by collecting TOF spectra at $m/e = 57$ ($C_4D_4H^+$) and $m/e = 56$ ($C_4D_3H_2^+$), which correspond to H loss and D loss from 1,3-butadiene-1,1,4,4-d_4; these TOF spectra are presented in Figure 2c,d. The C_3H_3 fragment from reaction R2 (methyl loss) was further investigated with TOF spectra for $m/e = 42$, 41, and 40 ($C_3D_3^+$, $C_3D_2H^+$, and $C_3DH_2^+$, respectively) at $\Theta_{LAB} = 15°$. These TOF spectra are presented in Figure 3d−f. For the methyl fragment, TOF spectra were collected for $m/e = 18$, 17, and 16 (CD_3^+, CD_2H^+, and CDH_2^+, respectively) at $\Theta_{LAB} = 15°$. For reaction R3, vinyl loss, spectra were collected for $m/e = 30$, 29, and 28 ($C_2D_3^+$, $C_2D_2H^+$, and $C_2DH_2^+$, respectively) at $\Theta_{LAB} = 15°$. The TOF spectrum for $m/e = 29$ ($C_2D_2H^+$) at $\Theta_{LAB} = 15°$ is presented in Figure 4c. No evidence for signal from reaction R3 was observed at $m/e = 30$ or 28.

For R4, molecular hydrogen loss, spectra were collected for $m/e = 56$ ($C_4D_4^+$) at $\Theta_{LAB} = 12°$ and 15°, as well as for $m/e = 55$ and 54 ($C_4D_3H^+$ and $C_4D_2H_2^+$, respectively) at $\Theta_{LAB} = 10°$ and 15°. TOF profiles for $m/e = 56$ ($C_4D_4^+$), 55 ($C_4D_3H^+$), and 54 ($C_4D_2H_2^+$) at $\Theta_{LAB} = 15°$ are presented in Figure 5c−e. Finally, for ethylene production (reaction R5), TOF spectra were collected for $m/e = 32$, 31, and 30 ($C_2D_4^+$, $C_2D_3H^+$, and $C_2D_2H_2^+$, respectively) at $\Theta_{LAB} = 15°$ and presented in Figure 6d−f. Additional TOF spectra were collected for $m/e = 28$, 27, and 26 ($C_2D_2^+$, C_2DH^+, and $C_2H_2^+$, respectively) at $\Theta_{LAB} = 15°$ (not shown).

B. TOF Spectra Collected Using Electron Impact. TOF spectra were collected on the EI instrument for $m/e = 54$ ($C_4H_6^+$), 53 ($C_4H_5^+$), 52 ($C_4H_4^+$), 51 ($C_4H_3^+$), 50 ($C_4H_2^+$), 49 (C_4H^+), 48 (C_4^+), 39 ($C_3H_3^+$), 38 ($C_3H_2^+$), 37 (C_3H^+), 36 (C_3^+), 28 ($C_2H_4^+$), 27 ($C_2H_3^+$), 26 ($C_2H_2^+$), 25 (C_2H^+), 24 (C_2^+), 15 (CH_3^+), 14 (CH_2^+), 13 (CH^+), and 12 (C^+). Spectra were not

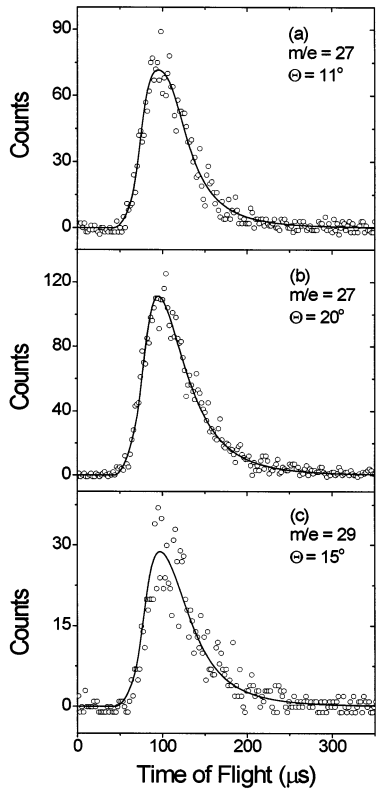

Figure 4. TOF spectra for $m/e = 27$ ($C_2H_3^+$) at source angles of (a) 11° at 9.5 eV with the MgF_2 window and (b) 20° at 11.0 eV. Also the TOF spectrum is shown for (c) $m/e = 29$ ($C_2D_2H^+$) from 1,3-butadiene-1,1,4,4-d_4 at $\Theta_{LAB} = 15°$ using 10.5 eV with the MgF_2 window. For all TOF spectra, the open circles represent the data and the solid line represents the forward convolution fit to the data using the $P(E_T)$ distribution shown in Figure 9c.

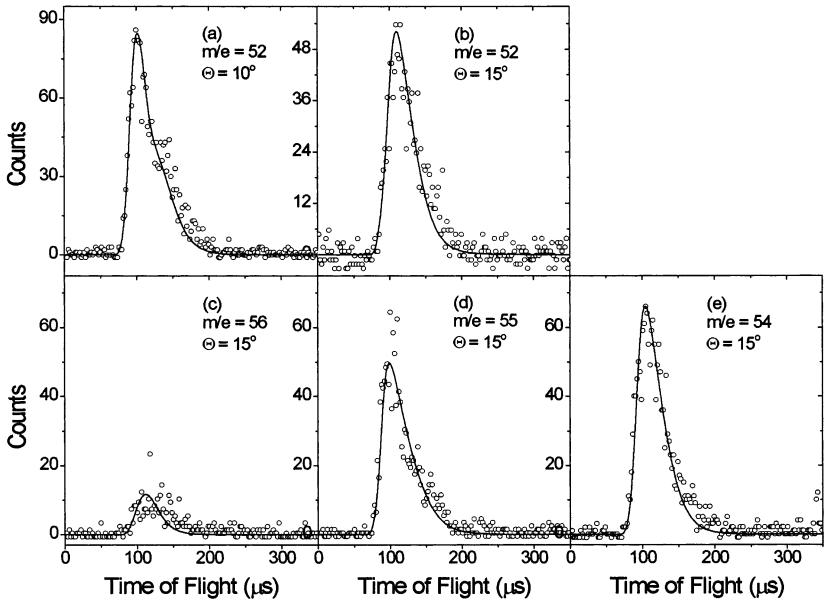

Figure 5. TOF spectra for $m/e = 52$ ($C_4H_4^+$) at source angles of (a) 10° at 10.0 eV with the MgF_2 window and (b) 15° at 11.5 eV. The open circles represent the data and the solid line represents the forward convolution fit to the data using the $P(E_T)$ distribution shown in Figure 10a. Also, TOF spectra for (c) $m/e = 56$ ($C_4D_4^+$), (d) $m/e = 55$ ($C_4D_3H^+$), and (e) $m/e = 54$ ($C_4D_2H_2^+$) from 1,3-butadiene-1,1,4,4-d_4 at $\Theta_{LAB} = 15°$ using 10.0 eV with the MgF_2 window. The open circles represent the data and the solid line represents the forward convolution fit to the data using the $P(E_T)$ distributions shown in Figure 11a for $m/e = 56$, in Figure 11b for $m/e = 55$, and in Figure 11c for $m/e = 54$.

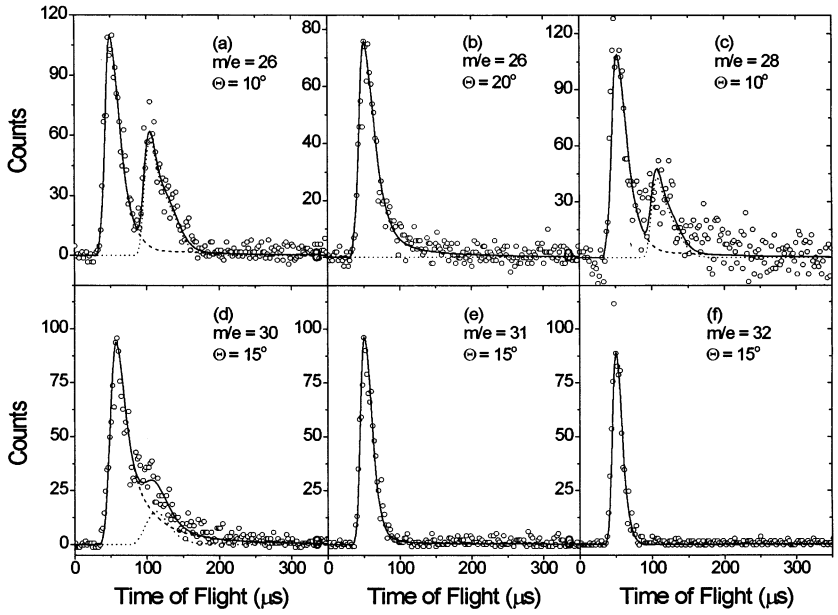

Figure 6. TOF spectra for $m/e = 26$ ($C_2H_2^+$) at source angles of (a) 10° and (b) 20° at 11.5 eV and for $m/e = 28$ ($C_2H_4^+$) at a source angle of (c) 10° at 12.0 eV. The open circles represent the data, the dashed line represents the forward convolution fit to the data using the $P(E_T)$ distribution shown in Figure 10b, the dotted line is the contribution from the $P(E_T)$ distribution in Figure 12a for dimer dissociation (see text), and the solid line is the sum of the dashed and dotted lines. TOF spectra are also shown for (d) $m/e = 30$ ($C_2D_2H_2^+$), (e) $m/e = 31$ ($C_2D_3H^+$), and (f) $m/e = 32$ ($C_2D_4^+$) from 1,3-butadiene-1,1,4,4-d_4 at $\Theta_{LAB} = 15°$ and 11.5 eV. Legends are the same as above except that dashed and solid lines are contributions from the $P(E_T)$ distributions shown in Figure 11d for $m/e = 32$, Figure 11e for $m/e = 31$, and Figure 11f for $m/e = 30$.

collected for $m/e = 28$ ($C_2H_4^+$), due to the prohibitive amount of background in the detector, or for $m/e = 2$ or 1, due to high background and poor kinematics. For $m/e = 53$ ($C_4H_5^+$), spectra were collected at $\Theta_{LAB} = 7°$ and 10°. For other values of m/e, spectra were collected at $\Theta_{LAB} = 7°$, 10°, and 15°. Additionally, spectra were collected for $m/e = 26$ ($C_2H_2^+$), $m/e = 25$ (C_2H^+), and $m/e = 24$ (C_2^+) at $\Theta_{LAB} = 20°$, and spectra were collected at $m/e = 51$ ($C_4H_3^+$) at $\Theta_{LAB} = 20°$ and 25°. To characterize the possible contribution of $(C_4H_6)_2$ parent dimer photodissociation to the product TOF spectra, spectra were collected for $m/e = 54$ ($C_4H_6^+$) at $\Theta_{LAB} = 7°$, 8°, 9°, 10°, and 15°. Figure 7 shows representative TOF spectra obtained using EI detection.

To appreciate the simplification of TOF spectra afforded by using tunable VUV undulator radiation, one should compare the $m/e = 27$ and 26 TOF spectra in Figures 4 and 6 with those presented in Figure 7e,f; the additional features in the latter spectra are the result of DI of higher mass products. Problems associated with DI should be even more severe for photodissociation of 1,3-butadiene-1,1,4,4-d_4, and no experiments on this compound were carried out on the EI instrument.

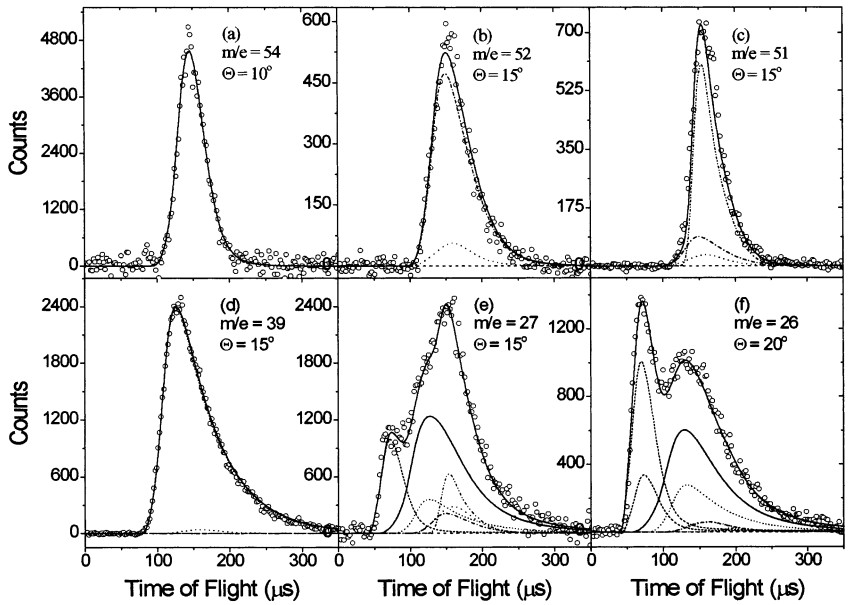

Figure 7. TOF spectra using electron impact detection for (a) $m/e = 54$ ($C_4H_6^+$) at $\Theta_{LAB} = 10°$, (b) $m/e = 52$ ($C_4H_4^+$) at $\Theta_{LAB} = 15°$, (c) $m/e = 51$ ($C_4H_3^+$) at $\Theta_{LAB} = 15°$, (d) $m/e = 39$ ($C_3H_3^+$) at $\Theta_{LAB} = 15°$, (e) $m/e = 27$ ($C_2H_3^+$) at $\Theta_{LAB} = 15°$, and (f) $m/e = 26$ ($C_2H_2^+$) at $\Theta_{LAB} = 20°$. The open circles represent the data and the solid line represents the forward convolution fit to the data using the $P(E_T)$ distributions shown in Figures 9, 10, and 12. The dashed line represents $m/e = 53$ ($C_4H_5^+$), the dotted line represents $m/e = 54$ ($C_4H_6^+$), the dash−dotted line represents $m/e = 52$ ($C_4H_4^+$), the dash−dot-dotted line represents $m/e = 51$ ($C_4H_3^+$), the short-dashed line represents $m/e = 39$ ($C_3H_3^+$), the short-dotted line represents $m/e = 27$ ($C_2H_3^+$), and the short-dash−dotted line is used for $m/e = 28$ ($C_2H_4^+$) as well as for $m/e = 26$ ($C_2H_2^+$). The $m/e = 28$ and $m/e = 26$ are easily differentiated in panel f by noting that the $m/e = 26$ contribution is larger than the $m/e = 28$ contribution.

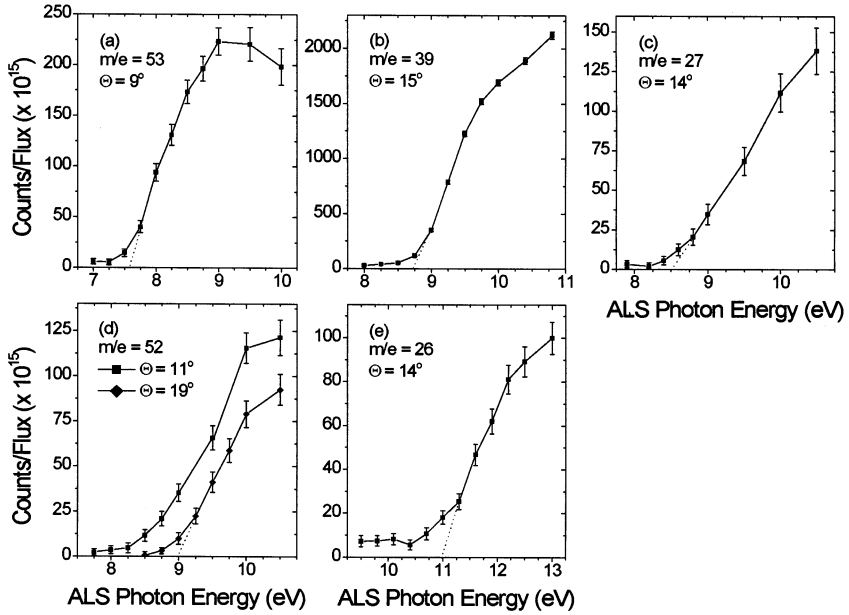

Figure 8. (a) Photoionization efficiency curve for $m/e = 53$ ($C_4H_5^+$) at a source angle of 9° for photoionization energies of 7.0−10.0 eV. (b) Photoionization efficiency curve for $m/e = 39$ ($C_3H_3^+$) at a source angle of 15° for photoionization energies of 8.0−10.8 eV. (c) Photoionization efficiency curve for $m/e = 27$ ($C_2H_3^+$) at a source angle of 14° for photoionization energies of 7.9−10.5 eV. (d) Photoionization efficiency curve for $m/e = 52$ ($C_4H_5^+$) at source angles of 11° for photoionization energies of 7.75−10.5 eV and 19° for photoionization energies of 8.5−10.5 eV. (e) Photoionization efficiency curve for $m/e = 26$ ($C_2H_2^+$) at a source angle of 14° for photoionization energies of 9.5−13.0 eV. The squares represent the data points with 2σ error bars. The MgF_2 window was in place during data collection for panels a−d.

C. PIE Measurements. PIE curves for several scattered photoproducts are shown in Figure 8. The PIE curve for scattered C_4H_5 fragments, shown in Figure 8a, was taken at $\Theta_{LAB} = 9°$ with the MgF_2 window in place. PIE curves were also obtained for C_4D_4H and $C_4D_3H_2$ fragments at $\Theta_{LAB} = 7°$ with the MgF_2 window in place and were very similar to that in Figure 8a. As seen in the figure, the photoionization onset for C_4H_5 is 7.3 ± 0.2 eV. The photoionization onsets for fragments from the deuterated species are 7.0 ± 0.2 eV for C_4D_4H and 7.3 ± 0.2 eV for $C_4D_3H_2$. In PIE curves, vibrational excitation of the recoiling photoproducts can produce hot bands that show up as "tails" extending to low photon energy. Straight-line extrapolation of the PIE curve can be used to provide a rough estimate of the ionization potential (IP) of the fragment. This procedure yields IPs of 7.6 ± 0.2 eV for C_4H_5 and its isotopomers. IPs have been derived by Lias et al.[4,10] for two isomers of C_4H_5, 1-butyn-3-yl (IP = 7.97 eV) and but-2-yn-1-yl (IP = 7.95 eV).

Figure 8b shows the PIE curve for C_3H_3 fragments at $\Theta_{LAB} = 15°$. The photoionization onset for $m/e = 39$ products is 8.0 ± 0.2 eV or lower; straight-line extrapolation yields an IP of 8.7 ± 0.2 eV. This value indicates that the C_3H_3 fragment is formed as the propargyl radical, for which the IP has been determined to be 8.673 eV using ZEKE spectroscopy.[9] The vertical IP for the propynyl radical was calculated to be ~11 eV,[47] and the IP for the cyclopropenyl radical has been reported to be 6.6 eV.[4] The PIE curve for C_2H_3 fragments at $\Theta_{LAB} = 14°$ is shown in Figure 8c. The photoionization onset for this fragment is 8.2 ± 0.2 eV, and straight-line extrapolation yields an IP of 8.5 ± 0.2 eV. Berkowitz et al. studied the photoionization spectra of the vinyl radical and determined an ionization threshold of 8.59 ± 0.03 eV.[48]

The PIE curves for C_4H_4 fragments at $\Theta_{LAB} = 11°$ and 19° are shown in Figure 8d. The PIE curve at 11° extends to considerably lower photon energies than does the PIE curve at 19°, indicating that C_4H_4 products at $\Theta_{LAB} = 11°$ are more vibrationally excited than at $\Theta_{LAB} = 19°$. This observation reflects the fact that, at larger angles, one is sampling fragments with more translational energy and less internal energy. Hence, the data at the larger angle should be used in any attempt to identify the C_4H_4 species, because these fragments will be colder than those at smaller angles. Thus, the IP extrapolated for these species will be closer to the true IP. The photoionization onset at $\Theta_{LAB} = 19°$ is 8.5 ± 0.2 eV, and straight-line extrapolation yields an IP of 9.0 ± 0.2 eV. The accepted values for the IPs for vinylacetylene, 1,2,3-butatriene, cyclobutadiene, and methylenecyclopropene are 9.58 ± 0.02, 9.15 ± 0.02, 8.16 ± 0.03, and 8.15 ± 0.03 eV (8.41 ± 0.05 eV vertical value), respectively.[10] Thus, the PIE curve at $\Theta_{LAB} = 19°$ suggests that the C_4H_4 fragment is either vinylacetylene or 1,2,3-butatriene.

Figure 8e shows the PIE curve for the C_2H_2 fragment from 1,3-butadiene dissociation at $\Theta_{LAB} = 14°$. PIE curves were also obtained for C_2DH and C_2H_2 fragments from 1,3-butadiene-1,1,4,4-d_4 dissociation at $\Theta_{LAB} = 14°$. The photoionization onsets are 10.4 ± 0.3 eV for C_2H_2 from 1,3-butadiene and 10.4 ± 0.3 eV for C_2DH and C_2H_2 from 1,3-butadiene-1,1,4,4-d_4. The straight-line extrapolated IPs for these species are 11.0 ± 0.3, 10.9 ± 0.3, and 11.2 ± 0.3 eV, respectively. In TOF spectra showing an additional slow peak (e.g., Figure 6a), only the fast feature in the spectrum was integrated. These values are reasonably close to the IP for acetylene, 11.400 ± 0.002 eV.[10]

Analysis

A. Translational Energy Distributions. In this section, translational energy distributions in the center-of-mass frame of reference are determined for the products of 1,3-butadiene photodissociation by fitting the TOF data obtained on the PI instrument; these data are much more straightforward to analyze than that obtained on the EI instrument because of minimal fragmentation from dissociation ionization.

For each channel, the total photofragment energy and angular distribution $P(E_T,\theta)$ is given by

$$P(E_T,\theta) = P(E_T)T(\theta) \quad (1)$$

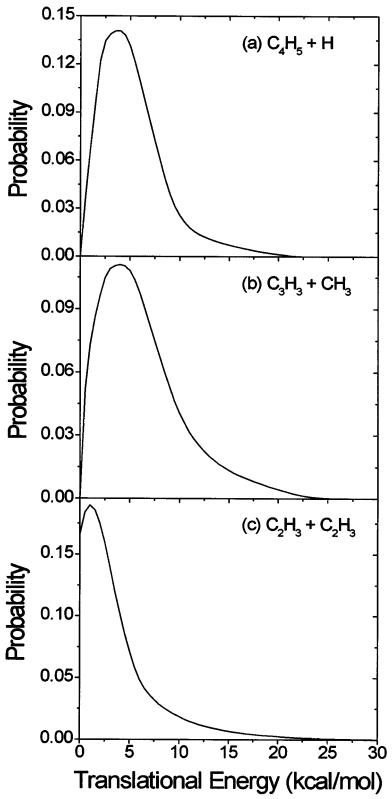

Figure 9. Center-of-mass (CM) translational energy distributions ($P(E_T)$ distributions) for (a) atomic hydrogen loss (R1), (b) methyl loss (R2), and (c) vinyl radical loss (R3).

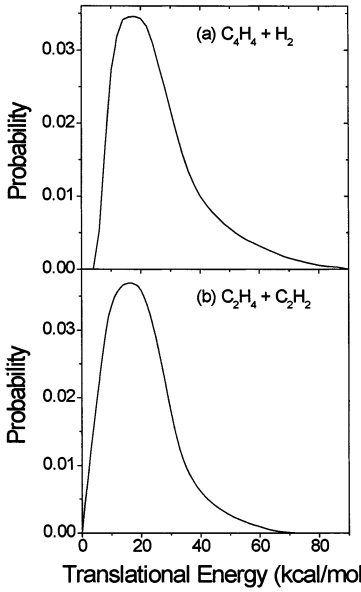

Figure 10. CM translational energy distributions for (a) molecular hydrogen loss (R4) and (b) ethylene loss (R5).

where $P(E_T)$ and $T(\theta)$ are the uncoupled center-of-mass frame translational energy and angular distributions, respectively. In the experiments described in this paper, the excimer laser is unpolarized, so with the rotating-source/fixed-detector geometry in the PI instrument, in which the laser propagation direction is perpendicular to the plane defined by the molecular beam and the detector, $T(\theta)$ for each channel is isotropic in the detection plane. For each channel, we determine the $P(E_T)$ distribution by forward convolution, in which an assumed $P(E_T)$ distribution

(47) Sun, W.; Yokoyama, K.; Robinson, J. C.; Suits, A. G.; Neumark, D. M. *J. Chem. Phys.* **1999**, *110*, 4363−4368.
(48) Berkowitz, J.; Mayhew, C. A.; Ruščic, B. *J. Chem. Phys.* **1988**, *88*, 7396−7404.

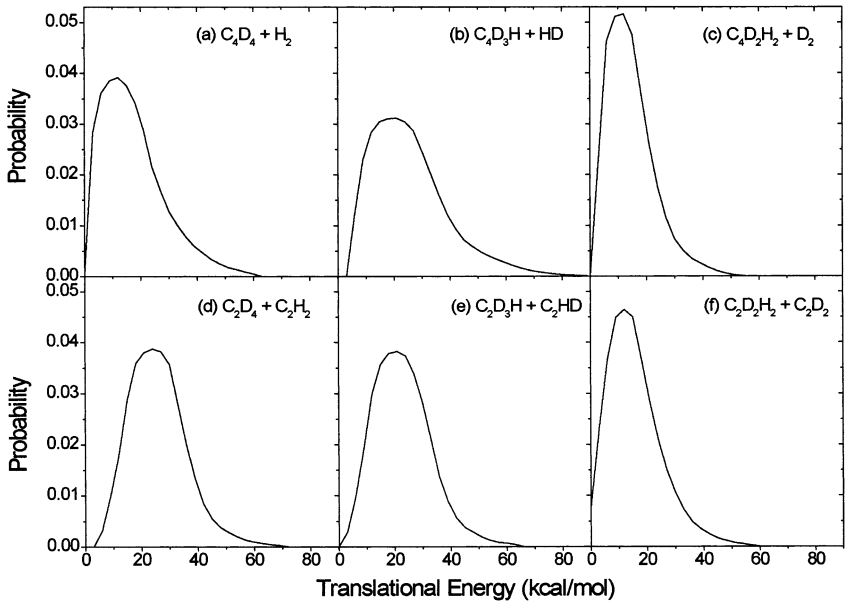

Figure 11. CM translational energy distributions for (a) $C_4D_4 + H_2$, (b) $C_4D_3H + HD$, and (c) $C_4D_2H_2 + D_2$ channels from 1,3-butadiene-1,1,4,4-d_4. Also, CM translational energy distributions for (d) $C_2D_4 + C_2H_2$, (e) $C_2D_3H + C_2DH$, and (f) $C_2D_2H_2 + C_2D_2$ channels from 1,3-butadiene-1,1,4,4-d_4.

Table 1. Relevant Quantities from CM Translational Energy Distributions Used To Fit the Laboratory Frame Data[a]

channel	$<E_T>$	E_{avl}	f_T	$E_{T,peak}$	$E_{T,max}$
R1: $C_4H_5 + H$	5.3	38.7	0.14	4	23
R2: $C_3H_3 + CH_3$	6.3	58.0	0.11	4	26
R3: $C_2H_3 + C_2H_3$	4.1	31.1	0.13	1	31
R4: $C_4H_4 + H_2$	26.1	103.7	0.25	18	90
R5: $C_2H_4 + C_2H_2$	20.2	107.4	0.19	16	72
R4: $C_4D_4 + H_2$	17.5	103.7	0.17	12	63
R4: $C_4D_3H + HD$	25.7	103.7	0.25	21	90
R4: $C_4D_2H_2 + D_2$	14.5	103.7	0.14	12	57
R5: $C_2D_4 + C_2H_2$	25.9	107.4	0.24	24	72
R5: $C_2D_3H + C_2DH$	22.9	107.4	0.21	21	66
R5: $C_2D_2H_2 + C_2D_2$	15.8	107.4	0.15	12	60

[a] All values for energies (denoted E) are in unites of kcal/mol.

is convoluted with the various instrument parameters to simulate the TOF spectra.[49,50] Point-wise adjustment of the $P(E_T)$ distribution is carried out until one obtains the best simultaneous fit of the simulated and experimental TOF spectra at all observed scattering angles. The $P(E_T)$ distributions are plotted in Figures 9−11 and summarized in Table 1, which presents the average translational energy release ($<E_T>$), the maximum available energy for each channel (E_{avl}), the fraction of energy released into translation (f_T), the value of E_T at the peak of the distribution ($E_{T,peak}$), and the maximum value of E_T in the distribution ($E_{T,max}$). In presenting E_{avl} and calculating f_T, we assumed the identity of the C_4H_5 fragment to be *i*-C_4H_5 (R1), the C_3H_3 fragment to be propargyl radical (R2), the C_4H_4 fragment to be vinylacetylene (R4), and the C_2H_2 fragment to be acetylene (R5).

The $P(E_T)$ distributions used to fit the radical channels R1−R3 are shown in Figure 9a−c. The simulated TOF spectra obtained from these distributions are shown as solid lines in Figures 2−4. The $P(E_T)$ distributions for the two molecular channels, $C_4H_4 + H_2$ (R4) and $C_2H_4 + C_2H_2$ (R5), are shown in Figure 10a and b, respectively, and the corresponding calculated simulated TOF distributions are superimposed on the data in Figures 5a,b and 6a−c. These $P(E_T)$ distributions are quite different from those for the radical channels, as they both peak at substantially higher values of translational energy. Note that the slow peaks in Figure 6a and c are not fit by the $P(E_T)$ distributions shown here; instead, they are attributed to dissociative ionization of C_4H_6 produced by photodissociation of the small amount of $(C_4H_6)_2$ in the beam. This issue is addressed in more detail below.

For 1,3-butadiene-1,1,4,4-d_4 dissociation, the TOF spectra for the radical channels in Figures 2−4 could be fit with the same $P(E_T)$ distributions used for the corresponding radical channels of 1,3-butadiene dissociation, regardless of the product masses. For example, the $m/e = 57$ and 56 TOF spectra in Figure 2c,d, corresponding to $C_4D_4H + H$ and $C_4D_3H_2 + D$, were both fit with the $P(E_T)$ distribution in Figure 9a. The situation for the molecular channels is more complicated. Figure 11a−c shows the $P(E_T)$ distributions for $C_4D_4 + H_2$, $C_4D_3H + HD$, and $C_4D_2H_2 + D_2$ that reproduced the laboratory TOF data at $m/e = 56$, 55, and 54, respectively. The $P(E_T)$ distributions for $m/e = 55$ and 54 are clearly different; the distribution for $C_4D_3H + HD$ is quite similar to the one in Figure 10a used to fit the $C_4H_4 + H_2$ channel, but the $C_4D_2H_2 + D_2$ distribution in Figure 10c peaks at lower translational energy. The $P(E_T)$ distribution for $m/e = 56$ is not as well determined as the other two due to the low S/N of the TOF spectrum. Figure 11d−f also presents the $P(E_T)$ distributions used to fit the $C_2D_4 + C_2H_2$, $C_2D_3H + C_2DH$, and $C_2D_2H_2 + C_2D_2$ data, respectively. The $P(E_T)$ distributions for $C_2D_4 + C_2H_2$ and $C_2D_3H + C_2DH$ are not identical but quite similar, while the distribution for $C_2D_2H_2 + C_2D_2$ peaks at a noticeably lower energy, 12 kcal/mol, versus over 20 kcal/mol for the other two.

The EI TOF spectra were fit using the $P(E_T)$ distributions obtained from analysis of the PI data. The EI data typically contain contributions from both the parent ion and fragment ions from dissociative ionization of higher mass channels; these data were fit by varying the weighting of each channel but *not* the form of the $P(E_T)$ distributions. When data were collected

(49) Zhao, X. Ph.D. Thesis, University of California, Berkeley, 1988.
(50) Myers, J. D. Ph.D. Thesis, University of California, Berkeley, 1993.

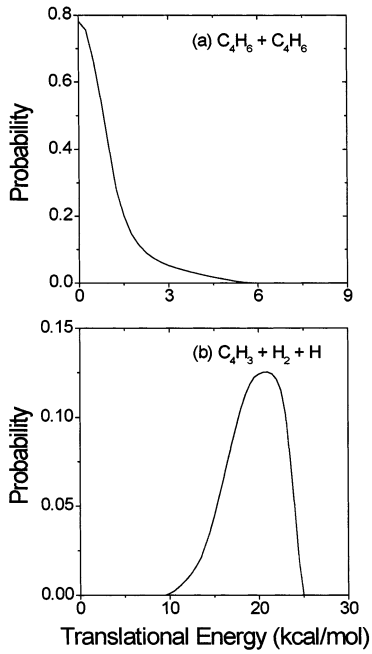

Figure 12. CM translational energy distributions for (a) $C_4H_6 + C_4H_6$ and (b) $C_4H_3 + H_2 + H$ obtained from electron impact studies.

at several scattering angles for a particular *m*/*e* value, this group of TOF spectra was fit using a single set of channel weightings. On the EI instrument, the detector rotates in the plane of the laser and molecular beams, so in principle an anisotropic product angular distribution, $T(\theta)$, can be observed even when an unpolarized laser is used.[51] However, we obtained a satisfactory fit to the data by assuming an isotropic distribution. Figure 7 shows representative fits of the EI TOF spectra, nearly of all of which have more than one channel contributing. In particular, the results at $m/e = 26$ and 27 are dominated by fragmentation and would have been extremely challenging to analyze in the absence of predetermined $P(E_T)$ distributions for each channel.

Analysis of the EI data revealed two additional contributions to the overall dynamics. Scattered photoproduct at $m/e = 54$, an example of which is shown in Figure 7a, cannot arise from photodissociation of C_4H_6. Instead, we assign this contribution to photodissociation of the small amount of $(C_4H_6)_2$ dimer in the parent molecular beam to form two monomers. The TOF data at $m/e = 54$ can be fit with the $P(E_T)$ distribution shown in Figure 12a; this distribution peaks at $E_T = 0$ and extends out to only 6 kcal/mol, indicating that one (or both) of the monomer products contains substantial internal excitation. Dissociative ionization from this channel contributes to several of the EI TOF spectra in Figure 7 for lower *m*/*e* (dotted line); these contributions can all be fit with the $P(E_T)$ distribution in Figure 12a. In the PI data set, the slow peaks in Figure 6 can also be fit by the $P(E_T)$ distribution in Figure 12a. We thus attribute these peaks to dissociative ionization of hot C_4H_6 products from dimer dissociation to form $C_2H_2^+$ and $C_2H_4^+$ at the relatively high VUV photon energies of 11.5 and 12.0 eV used in obtaining the data in Figure 6. All the other TOF spectra in Figures 2−6 were taken at either lower ionization energies, where no DI of C_4H_6 occurs, or larger scattering angles, where there is less contribution from dimer dissociation.

The EI TOF spectra show an additional channel that was not investigated in the PI experiments. Data at $m/e = 51$, an example of which is shown in Figure 7c, could not be fit by assuming only dissociative ionization of heavier products, indicating a contribution from a neutral product with mass 51, i.e., C_4H_3. This product cannot be formed in a single, two-body process, but it could arise from the production of vibrationally excited C_4H_4* via R4, which then undergoes spontaneous dissociation to $C_4H_3 + H$:

$$C_4H_6 \xrightarrow{h\nu} C_4H_4^* + H_2 \rightarrow C_4H_3 + H + H_2 \qquad (R4^*)$$

According to a computational study by Miller and Melius, the lowest energy C_4H_3 structure is *i*-C_4H_3 (H_2CCCCH) with a heat of formation of 111.3 ± 15.9 kcal/mol.[6] Given this heat of formation and others from the literature,[10] production of *i*-C_4H_3 is energetically feasible at 193 nm through R4*. Since the second step of R4* involves loss of a relatively slow H atom, the laboratory velocity distribution for the C_4H_3 product should be similar to that of the C_4H_4* precursor. Hence, the mass 51 contribution to the TOF data was fit using the two-body $P(E_T)$ distribution in Figure 12b by assuming mass 52 + 2 products; essentially, this is the $P(E_T)$ distribution for those C_4H_4 products with sufficient internal energy to undergo further dissociation. This distribution resembles the slow part of the $P(E_T)$ distribution for R4 in Figure 10a, consistent with our expectation that the slowest C_4H_4 products are the likeliest to lose an H atom.

B. Branching Ratios. The fitting program used to simulate the TOF spectra from the $P(E_T)$ distributions provides the weighting for each $P(E_T)$ distribution that is required to reproduce the relative signal intensity in the TOF spectra for each channel.[50] By normalizing these weightings to the number of laser shots, average laser power, total number of counts in the TOF spectra, and (in the PI experiment) VUV flux, one obtains "apparent" relative cross sections σ_k^0, where $k = m/e$ for the detected ion fragment. Conversion of the apparent cross sections into branching ratios using the PI data requires knowledge of absolute PI cross sections at the photon energies used in our experiment. Unfortunately, these are unknown for most of the products from reactions R1−R5.

On the other hand, electron impact ionization cross sections can be estimated, as described in detail by Schmoltner[52] for the instrument used in this study. Electron impact ionization cross sections were calculated using the additivity rule proposed by Fitch and Sauter[53] as explained by Schmoltner.[52] Briefly, the electron impact cross section (in units of 10^{-16} cm^2) is estimated from the following additivity formula:

$$Q = 0.082 + \sum_{i=1} a_i n_i \qquad (2)$$

which was obtained from a least-squares fit to a total of 179 ionization cross sections from the literature. The atomic cross sections are $a_i = 1.43 \times 10^{-16}$ cm^2 for carbon and $a_i = 0.73 \times 10^{-16}$ cm^2 for hydrogen, and n_i represents the number of atoms of type *i* in the molecule. The major source of error in this approximation is the experimental error in the cross section determinations, which was approximately 10−20%.[52]

(51) Hayden, C. C.; Neumark, D. M.; Shobatake, K.; Sparks, R. K.; Lee, Y. T. *J. Chem. Phys.* **1982**, *76*, 3607−3613.

(52) Schmoltner, A. M. Ph.D. Thesis, University of California, Berkeley, 1989.
(53) Fitch, W. L.; Sauter, A. D. *Anal. Chem.* **1983**, *55*, 832−835.

Table 2. Branching Ratios for Product Channels from the Dissociation of 1,3-Butadiene at 193 nm

channel	contribution
R1: $C_4H_5 + H$	20
R2: $C_3H_3 + CH_3$	50
R3: $C_2H_3 + C_2H_3$	8
R4: $C_4H_4 + H_2$	2[a]
R5: $C_2H_4 + C_2H_2$	20

[a] The $m/e = 52$ contribution does not include the product that appears at $m/e = 51$. The ratio of $m/e = 51$ to $m/e = 52$ product is 1.6:1.

The fraction of product in channel i, R_i, is given by

$$R_i = \sigma_i / \sum_j \sigma_j \tag{3}$$

where

$$\sigma_i = \frac{1}{Q_i} \sum_{k=m/e} \frac{\sigma_k^0}{T_k} \tag{4}$$

Here σ_i is the relative cross section for the neutral photoproduct i, Q_i is the ionization cross section from eq 2, the index k refers to the m/e values of the parent and fragment ions produced in the ionizer from this photoproduct, σ_k^0 is the suitably normalized apparent cross section obtained from our fitting procedure for production of ionic fragment k needed to fit the TOF spectra at $k = m/e$, and T_k is the relative quadrupole transmission function for ions of mass-to-charge ratio $k = m/e$. The T_k term is assumed to be linear with mass and was determined by requiring the relative cross sections for the momentum-matched products CH_3 and C_3H_3 to be equal. In practice, the correction for T_k is on the order of 10%; the equation for T_k is dominated by the y-intercept, while the slope term represents a small correction. Note that use of eq 4 requires measurement of TOF spectra at all possible fragment masses for each primary channel, because the fragmentation patterns for many of the radical products are not known a priori; this requirement explains the necessity for measuring so many TOF spectra on the EI instrument, as described in the section on TOF Spectra Collected Using Electron Impact.

The branching ratios obtained from eqs 3 and 4 are shown in Table 2. Reaction R2, the production of $C_3H_3 + CH_3$, is the dominant channel, followed by R1 and R5, which have comparable branching ratios. We estimate error bars of 25%, based on the uncertainties in the electron impact cross sections, Q_i. Signal from dimer dissociation contributes 2% to the total scattering, and ~60% of the primary product C_4H_4 undergoes spontaneous loss of an H atom via R4*.

Additionally, branching ratios were determined for the products of 1,3-butadiene-1,1,4,4-d_4 photodissociation. In this case, we were interested in the isotopic distribution of products *within* each primary channel R1−R5. Therefore, we were able to use the PI data, since these distributions are independent of photoionization cross section as long as the same photon energy is used for each primary channel. The appropriate $P(E_T)$ distributions for each isotopomer were used, and all TOF spectra were normalized to the VUV flux. The relative branching ratios within each channel are shown in Table 3, which includes some experimental details. For reaction R1, which corresponds to H loss, laboratory TOF data were used for $m/e = 57$ ($C_4D_4H^+$) and $m/e = 56$ ($C_4D_3H_2^+$) at $\Theta_{LAB} = 7°$. For reaction R2, methyl loss, TOF spectra for $m/e = 42$, 41, and 40 ($C_3D_3^+$, $C_3D_2H^+$, and $C_3DH_2^+$, respectively) at $\Theta_{LAB} = 15°$ were used since their S/N ratios were superior to those of the methyl TOF spectra. TOF spectra exhibited evidence for R3, central C−C cleavage to yield two vinyl radicals, only at $m/e = 29$ ($C_2D_2H + C_2D_2H$). For R4, molecular hydrogen loss TOF spectra were used for $m/e = 56$ (H_2 loss) at $\Theta_{LAB} = 15°$ and for $m/e = 55$ and 54 (HD and D_2 loss, respectively) at $\Theta_{LAB} = 10°$ and 15°. Finally, for reaction R5, TOF spectra for $m/e = 32$, 31, and 30 ($C_2D_4^+$, $C_2D_3H^+$, and $C_2D_2H_2^+$, respectively) were chosen for the fit. These "intrachannel" branching ratios should be more accurate than those in Table 2, with error bars of 10−15%.

Table 3. Relative Branching Ratios for Product Channels from the Dissociation of 1,3-Butadiene-1,1,4,4,-d_4 at 193 nm

channel	photoionization energy (eV)	contribution
R1: $C_4D_4H + H$	8.5	56
R1: $C_4D_3H_2 + D$	8.5	44
R2: $C_3D_3 + CDH_2$	10.5	10
R2: $C_3D_2H + CD_2H$	10.5	81
R2: $C_3DH_2 + CD_3$	10.5	9
R3: $C_2D_2H + C_2D_2H$	10.5	100
R4: $C_4D_4 + H_2$	10	9
R4: $C_4D_3H + HD$	10	27
R4: $C_4D_2H_2 + D_2$	10	64
R5: $C_2D_4 + C_2H_2$	11.5	32
R5: $C_2D_3H + C_2DH$	11.5	39
R5: $C_2D_2H_2 + C_2D_2$	11.5	29

Discussion

Figure 1 presented the various reaction channels that are possible for 1,3-butadiene dissociation following 193-nm excitation. In contrast to the 193-nm dissociation of 1,2-butadiene,[39] where only H atom loss and methyl loss (the dominant channel) were observed, five distinct reaction channels, R1−R5, are evident for the 193-nm dissociation of 1,3-butadiene. The $P(E_T)$ distributions for each of the three radical channels, R1−R3, peak at low translational energy (below 5 kcal/mol), while those for the two molecular channels, R4 and R5, peak at considerably higher barriers around 20 kcal/mol. These results are consistent with a mechanism in which photoexcitation is followed by internal conversion to the ground electronic state. Under these circumstances, the reaction coordinates for the various radical channels do not have exit barriers with respect to separated products; i.e., there are no barriers to the reverse radical recombination reactions. The resulting $P(E_T)$ distributions would then be approximately described by phase space theory or other statistical models, resulting in relatively little of the available energy appearing as translation, which is in agreement with the observed distributions. On the other hand, the $P(E_T)$ distributions for the molecular channels suggest these products involve passage over a substantial exit barrier, on the order of 1−2 eV with respect to the separated products. Again, this is what one would expect for ground-state dissociation in which dissociation to molecular products would proceed through a tight transition state atop a fairly large barrier. Hence, our results support the conclusion from previous spectroscopic and theoretical work, discussed in the Introduction, that rapid internal conversion to the ground state occurs prior to any dissociation.

Nonetheless, our results still raise several questions that need to be addressed. First, we need to understand the detailed mechanism for the various channels, some of which can occur by simple bond fission, while others appear to involve isomerization to another stable C_4H_6 structure prior to dissociation. Thus, even though the dissociation dynamics most likely occur on the ground electronic state, the dynamics on this state may be quite complicated. The isotopic studies are particularly helpful in this regard since they enable us to track the H atoms to some extent as the dynamics unfold. Second, we want to understand the considerable differences between the photochemistry of 1,3-butadiene and 1,2-butadiene. Finally, we compare our results to the earlier photolysis and pyrolysis experiments on 1,3-butadiene. In the following sections, each channel is covered in some detail, followed by a more general discussion.

A. R1: $C_4H_5 + H$. There are two inequivalent C−H bonds that can undergo fission in 1,3-butadiene. Loss of atomic hydrogen from either terminal carbon atom will produce the *n*-C_4H_5 radical, whereas atomic hydrogen loss from either central carbon atom will produce the *i*-C_4H_5 species. In an extensive investigation of the C_4H_5 isomers, Parker and Cooksey[7] found the *i*-C_4H_5 species to be either a shallow local minimum or a saddle point on the C_4H_5 potential energy surface. However, *i*-C_4H_5 can relocalize to 1,2-butadien-4-yl, a structure that is both stable and lower in energy. The *n*-C_4H_5 species was found to be roughly 2 kcal/mol higher in energy than the *i*-C_4H_5 species; the *n*-C_4H_5 species is a stable point on the global C_4H_5 potential energy surface. A statistical dissociation mechanism would favor H loss from the *i*-site, although one might expect loss from both sites to occur because these two C_4H_5 isomers are so close energetically. Photodissociation of 1,3-butadiene-1,1,4,4-d_4 yielded an H-to-D loss branching ratio of 56:44. Given that there are twice as many D's as H's in 1,3-butadiene-1,1,4,4-d_4, this finding indeed suggests that atomic H elimination from the *i*-site is favored.

Our study of 1,2-butadiene showed that the $P(E_T)$ distribution for the $C_4H_5 + H$ channel had to be truncated below $E_T = 7$ kcal/mol.[39] This observation was attributed to secondary decomposition of highly internally excited C_4H_5 products. No evidence for this process is seen for 1,3-butadiene; with the beam seeded in neon, taking beam velocity spread into account, we can detect products with as little as 2.5 kcal/mol translational energy at $\Theta_{LAB} = 9°$. The absence of secondary decomposition is consistent with the overall thermodynamics for this system. The heat of formation of 1,3-butadiene is 13 kcal/mol lower than that of 1,2-butadiene,[10] so secondary dissociation of the C_4H_5 product to H + vinylacetylene or $C_2H_3 + C_2H_2$ is not energetically possible at 193-nm excitation.

B. R2: $C_3H_3 + CH_3$. The dominant channel in this study, R2 ($CH_3 + C_3H_3$), is also the lowest energy radical channel. This channel lies 19.3 kcal/mol below the lowest simple bond fission channel to *i*-$C_4H_5 + H$ and 26.9 kcal/mol below the central C−C bond fission channel R3. However, R2 can proceed by bond fission only if isomerization to 1,2-butadiene occurs prior to dissociation, as was postulated in early photochemistry studies of 1,3-butadiene.[24,27] The translational energy distribution for this channel is similar to the distribution for $CH_3 + C_3H_3$ production from 1,2-butadiene dissociation at 193 nm,[39] although, as expected from energetic considerations, slightly less translational energy is released here than in the case of 1,2-butadiene dissociation. Moreover, our isotopic studies on 1,3-butadiene-1,1,4,4-d_4 show that 80% of the methyl loss channel appears as $CD_2H + C_3D_2H$, the expected product from 1,2-butadiene produced by an H atom shifting from C3 to C1. Hence, our results support the idea that this channel is indeed produced by isomerization to 1,2-butadiene followed by C−C bond fission. We do observe ~10% each of CD_3 and CDH_2 products, indicative of some H/D scrambling; the exact mechanism for formation of these products is as yet unclear.

C. R3: $C_2H_3 + C_2H_3$. R3 can occur by simple bond fission of the C2−C3 single bond, with no isomerization required. The $P(E_T)$ distribution for this channel is consistent with bond fission. Moreover, in the photodissociation of 1,3-butadiene-1,1,4,4-d_4, only mass 29 products, corresponding to C_2D_2H, are seen for this channel, indicating bond fission with no H/D scrambling. Breaking the C−C single bond is energetically less favorable than breaking either C−H bond (see Figure 1), leading to the R1/R3 branching ratio of 20:8.

D. R4: $C_4H_4 + H_2$. R4 can occur by several distinct dynamical pathways. The stable C_4H_4 products, vinylacetylene (H−C≡C−CH═CH_2) and 1,2,3-butatriene (H_2C═C═C═CH_2), can be formed via four-center transition states involving C1/C2 and C2/C3, respectively. Loss of two terminal H atoms via a three-center transition state would produce singlet vinylvinylidene (:C═CH−CH═CH_2), a species observed by Gunion et al.[54] in the photoelectron spectrum of $C_4H_4^-$; their calculations showed the neutral to have a very low isomerization barrier to the more stable vinylacetylene species. All three pathways involve a tight transition state and a substantial barrier with respect to products, consistent with the observed $P(E_T)$ distributions. As discussed in the section PIE Measurements, the PIE curves in Figure 8 are consistent with either stable C_4H_4 product.

The deuterated studies provide more insight into the dissociation mechanisms. We find that H_2 loss, HD loss, and D_2 loss occur with branching ratios of 9:27:64, similar to much earlier photolysis results obtained by Haller and Srivinvasan,[27] and implying that all three processes occur. The most probable of these processes is formation of vinylvinylidene through a three-center transition state. While it is possible that some isotopic scrambling occurs, the three $P(E_T)$ distributions in Figure 11a−c are different, with $\langle E_T \rangle = 17.5$, 25.7, and 14.5 kcal/mol for H_2 loss, HD loss, and D_2 loss, respectively, offering further support for the occurrence of three distinct channels. The maximum translational energy, $E_{T,max} = 57$ kcal/mol, in the $P(E_T)$ distribution for the D_2 loss channel is noticeably lower than in the other two distributions, consistent with forming the least stable product, i.e., vinylvinylidene. More quantitatively, the CISD calculations performed by Gunion et al.[54] yield a heat of formation for vinylvinylidene of 113.0 kcal/mol, 42.6 kcal/mol above vinylacetylene, resulting in an available energy of 61.1 kcal/mol for the products formed in this channel following dissociation. This value is higher than the experimental $E_{T,max}$ for D_2 loss, so our $P(E_T)$ distribution is consistent with vinylvinylidene production. Thus, our branching ratios and $P(E_T)$ distributions suggest that the barrier for the three-center transition state leading to this product is lower than those for the two four-center transition states leading directly to stable

(54) Gunion, R. F.; Köppel, H.; Leach, G. W.; Lineberger, W. C. *J. Chem. Phys.* **1995**, *103*, 1250−1262.

products. This three-center transition state is quite symmetric and should lead to relatively little H_2 rotational excitation but some H_2 vibrational excitation, consistent with the H_2 (v, J) distribution from 1,3-butadiene dissociation observed by Valentini.[38] Overall, R4 is a fascinating but almost insignificant part of the whole dissociation process.

E. R5: $C_2H_4 + C_2H_2$. Reaction R5 is the dominant molecular channel, comparable to the radical channel R1. In modeling their shock tube results on the pyrolysis of 1,3-butadiene, Hidaka et al.[35] assumed an activation energy of 77.1 kcal/mol for R5 with no discussion of the reaction mechanism. The detailed mechanism is of interest, since production of $C_2H_4 + C_2H_2$ requires some rearrangement prior to dissociation. The branching ratios in Table 3 and the $P(E_T)$ distributions in Figure 11d−f for the various product isotope combinations of this channel from the photodissociation of butadiene-1,1,4,4-d_4 show that multiple mechanisms are operative. Our branching ratio of 32:39:29 for $C_2D_4/C_2D_3H/C_2D_2H_2$ is similar to that obtained by Haller and Srinivasan,[27] indicating that their results, obtained at relatively high pressures (i.e., several Torr), were unperturbed by effects due to secondary collisions. They attributed the $C_2D_4 + C_2H_2$ channel to formation and subsequent dissociation of cyclobutene, the $C_2D_3H + C_2HD$ to a four-center transition state involving 1,3 D atom migration and dissociation of the C2−C3 single bond, and the $C_2D_2H_2 + C_2D_2$ channel to 3,1 H atom migration followed by dissociation to CD_2HCH (ethylidene) + $:C_2D_2$ (vinylidene), with the two fragments rapidly rearranging to $C_2D_2H_2 + C_2D_2$.

Our results support the main features of their proposed mechanisms for this channel. The three $P(E_T)$ distributions in Figure 11d−f are all different, indicating that each isotopic combination is produced by a different dynamical pathway. The $P(E_T)$ distribution for $C_2D_2H_2 + C_2D_2$ peaks at considerably lower energy than that for the other two isotopic combinations, consistent with the formation of high-energy products. However, formation of the two high-energy products as postulated by Haller is not energetically feasible at 193 nm, using $\Delta H_f = 99$ kcal/mol for vinylidene[5] and 73 kcal/mol for ethylidene.[55] Instead, this channel could result from a 2,3 H atom shift followed by dissociation to $CD_2CH_2 + :C_2D_2$. We can also comment further on the proposed cyclobutene mechanism. The activation energy for the reverse isomerization process, i.e., ring-opening cyclobutene, is 32.9 kcal/mol.[56] Based on the known heats of formation of cyclobutene (37.5 kcal/mol) and 1,3-butadiene (26.0 kcal/mol), the barrier to cyclobutene formation lies only 44.4 kcal/mol above *trans*-1,3-butadiene, so cyclobutene is certainly energetically accessible at our photon energy of 148.1 kcal/mol. The barrier for concerted dissociation to ethylene and acetylene has been calculated to lie 113 kcal/mol above cyclobutene,[57] i.e., 125 kcal/mol above 1,3-butadiene. It is unlikely that R5 would have a branching ratio more than twice that of R3 with a barrier of this height, so stepwise dissociation of the two bonds probably provides a lower energy pathway to products.

F. Comparison with Other Experiments. The 193-nm dissociation dynamics of 1,3-butadiene and 1,3-butadiene-1,1,4,4-d_4 differ markedly from those seen for 1,2-butadiene dissociation.[39] At 193 nm, 1,2-butadiene dissociation results in only two channels, atomic hydrogen loss and methyl loss, with methyl loss dominating. Both of these channels are simple bond fission channels. Hence, it appears that no isomerization from 1,2-butadiene to 1,3-butadiene occurs, because if it did, the molecular channels R4 and R5 along with the C−C bond fission channel R3 would have been seen. On the other hand, the observation of $CH_3 + C_3H_3$ (R2) as a major channel from 1,3-butadiene photodissociation implies that 1,3-butadiene does undergo significant isomerization to 1,2-butadiene.

These results can be understood based on the dissociation energetics in Figure 1 and the less well-known isomerization barriers. The prevalence of channel R2 over the C−C and C−H bond fission channels shows that passage over the tight transition state associated with isomerization to 1,2-butadiene is faster than direct bond fission. This situation can arise only if the barrier associated with the tight transition state is considerably lower than the bond dissociation energies for the C−C and lowest C−H bond fission channels from 1,3-butadiene (see Figure 1). Similarly, the prevalence of channel R5 over C−C bond fission shows that passage over the tight transition states associated with the molecular channel R5 is faster than direct C−C bond fission and that the barriers to channel R5 are lower than the bond dissociation energy for C−C bond fission. The shock tube results by Hidaka et al.[35] were modeled by assuming activation energies of only 75 kcal/mol for the 1,3-butadiene → 1,2-butadiene isomerization reaction and 77.1 kcal/mol for the production of $C_2H_4 + C_2H_2$, fairly consistent with our arguments, but clearly it would be useful to apply electronic structure calculations to these reaction paths to learn more about the barrier heights.

Comparison of the results for 1,2- and 1,3-butadiene indicates that once isomerization to 1,2-butadiene occurs, dissociation to $CH_3 + C_3H_3$ is considerably faster than the back reaction to reform 1,3-butadiene. This irreversibility of the isomerization reaction can be attributed to the relatively low bond dissociation energy of 1,2-butadiene to form $CH_3 + C_3H_3$, 77 kcal/mol. Thus, it appears that dissociation through the loose transition state associated with this bond fission process dominates over the back reaction through the tight isomerization transition state to 1,3-butadiene, which is a reasonable result from statistical theories of reaction dynamics when the excitation energy is well above both transition states.[58]

It is also of interest to compare our results with previous pyrolysis studies of 1,3-butadiene. As discussed in the Introduction, the interpretation of these shock tube studies requires extensive modeling because of the presence of secondary reactions and the difficulties in directly detecting many of the products. The most comprehensive study to date, by Hidaka et al.,[35] showed that R2 and R5 were the dominant dissociation channels and that, under the conditions of their experiment, reactions R1 and R3 were ∼2 orders of magnitude slower. Our results in Table 2, on the other hand, show that R1/R2/R3/R4/R5 is 20:50:8:2:20. These results are not inconsistent, because the average excitation energy in the shock tube experiments is considerably lower than in our experiments; at $T = 1500$ K, for example, nkT is ∼70 kcal/mol for C_4H_6, where $n = 24$ is

(55) Schultz, R. H.; Armentrout, P. B. *Organometallics* **1992**, *11*, 828−836.
(56) Carr, R. W.; Walters, W. D. *J. Phys. Chem.* **1965**, *69*, 1073−1075.
(57) Hess, B. A.; Schaad, L. J.; Reinhoudt, D. N. *Int. J. Quantum Chem.* **1986**, *29*, 345−350.
(58) Krajnovich, D.; Huisken, F.; Zhang, Z.; Shen, Y. R.; Lee, Y. T. *J. Chem. Phys.* **1982**, *77*, 5977−5989.

the number of vibrational degrees of freedom. This amount of energy is less than half the photon energy used in our work, and in any case, it represents an overestimate of the vibrational energy, because the high-frequency C−H stretches will not be excited at 1500 K. Hence, one would expect a higher yield from the high-energy bond fission processes R1 and R3 in our experiment. Our results agree with those of Hidaka et al.[35] on the point of central C−C bond cleavage to produce two vinyl radicals. Neither study finds vinyl loss to be a dominant channel; in the current study, we find vinyl loss to be about two-fifths as important as atomic hydrogen loss. Thus, we concur with Hidaka et al. that the omission of the isomerization process of 1,3-butadiene to 1,2-butadiene in the modeling of earlier pyrolysis studies[31,32] led to the erroneous conclusion that vinyl loss dominated this reaction.

Conclusions

Our results on the photodissociation dynamics of 1,3-butadiene at 193 nm show that this species exhibits rich and complex photochemistry. We observe five primary photochemical channels, three of which involve formation of two radical fragments and two of which result in molecular fragments. Branching ratio measurements indicate that the dominant channel is $CH_3 + C_3H_3$, followed by $C_4H_5 + H$ and $C_2H_4 + C_2H_2$, which are comparable in importance, followed by $C_2H_3 + C_2H_3$ and a very small amount of $C_4H_4 + H_2$. The observed $P(E_T)$ distributions suggest that all channels result from ground-state dissociation dynamics, because the distributions for the radical channels peak near $E_T = 0$ kcal/mol, while those for the molecular channels peak at considerably higher energies, indicating substantial exit barriers with respect to the products. The observation of ground-state dynamics is consistent with recent spectroscopic and theoretical studies that suggest that photoexcitation of 1,3-butadiene is followed by very rapid internal conversion to the ground state via conical intersections. Several of the observed channels involve isomerization prior to dissociation, and our studies of 1,3-butadiene-1,1,4,4-d_4 enable us to track the interplay between isomerization and dissociation on the ground-state surface.

Acknowledgment. This work was supported by the Director, Office of Basic Energy Sciences, Chemical Sciences Division of the U.S. Department of Energy under Contract DE AC03-76SF00098. J.C.R. would like to thank Prof. David Blank for providing his data from previous experiments on 1,3-butadiene at the ALS as well as for several helpful conversations. Furthermore, J.C.R. would like to thank Dr. Steven Harich and Prof. Xueming Yang of the Academia Sinica for generously providing an excellent program for forward convolution analysis. The authors acknowledge Prof. Tomas Baer and Prof. Arthur Suits for the use of End Station 1 on the Chemical Dynamics Beamline and Drs. Fei Qi and O. Sohrkabi for support during the initial experiments.

JA0127281